Accepted Manuscript – Final publication in Acta Materialia 165, 409-419, 2019

Anneal hardening and elevated temperature strain rate sensitivity of nanostructured metals: Their relation to intergranular dislocation accommodation

O. Renk [1*)], V. Maier-Kiener [2)], I. Issa [3)], J.H. Li [4)], D. Kiener [3)], R. Pippan [1)]

1) Erich-Schmid-Institute of Materials Science, Austrian Academy of Sciences, Jahnstrasse 12, 8700 Leoben, Austria

2) Department Physical Metallurgy and Materials Testing, Montanuniversität Leoben, Roseggerstrasse 12, 8700 Leoben, Austria

3) Department of Material Physics, Montanuniversität Leoben, Jahnstrasse 12, 8700 Leoben, Austria

4) Institute of Casting Research, Montanuniversität Leoben, Franz-Josef-Strasse 18, 8700 Leoben, Austria

*) corresponding author: Email: oliver.renk@oeaw.ac.at; Tel. 0043/3842 804 310

Keywords: ultrafine-grained; nanocrystalline; hardening; high temperature nanoindentation, severe plastic deformation; high pressure torsion

Abstract

Nanocrystalline materials exhibit various properties or phenomena not common in the conventional grain size regime, including enhanced strain rate sensitivity for FCC metals or strength increase during recovery annealing. These peculiarities are associated with the enhanced confinement of plasticity. Accordingly, the interaction of dislocations with the numerous grain boundaries, the boundary state as well as its local chemistry are of importance for a complete understanding. Due to the various influencing factors, determination of the dominant and rate controlling processes remains challenging. Here, we present a study on selected nanostructured FCC materials where dislocation-grain boundary interactions have been studied earlier for their coarse grained counterparts. High temperature nanoindentation revealed for all materials a pronounced increase of strain rate sensitivity when exceeding a certain temperature, peaking prior to the occurrence of significant grain growth. Static annealing of samples close to these peak temperatures leads, for sufficiently small grain sizes, to a maximum hardness increase. Interestingly, despite the nanocrystalline grain size, these temperatures perfectly agree with those obtained earlier for annihilation of lattice dislocations at grain boundaries in coarse-grained samples. This suggests that at elevated temperatures the dominant mechanism controlling the enhanced rate sensitivities in nanocrystalline metals is the thermally activated annihilation of lattice dislocations at grain boundaries. Measurements of activation energies being close to reported values for grain boundary diffusion further support this concept.

Published version available at http://dx.doi.org/10.1016/j.actamat.2018.12.002

1) Introduction

Besides the enormous strength increase achievable by reducing the grain size of polycrystals to dimensions well below one micrometer, several phenomena not accessible in their coarse grained (CG) counterparts are observed. For instance, the strength of nanostructured metals can increase rather than decrease when subjected to recovery annealing treatments [1–4]. Apart from that, for FCC metals an enhanced strain rate sensitivity (SRS) compared to CG samples was frequently reported [5–7]. Since these phenomena are already observed in the submicrometer range, they do not necessarily arise from deformation mechanisms subject to change, but due to the different nature of dislocation slip in these fine-grained specimens. In CG materials dislocations are continuously produced from intragranular sources, stored and rearranged during plastic deformation, subdividing the original crystal [8,9]. Such dislocation cells have typical sizes in the range of several 100 nm, depending on material and deformation conditions [9,10]. For this reason, in CG crystals the majority of processes during plastic deformation typically occur within the grain or cell interior, leading mainly to dislocation-dislocation interactions. This is also reflected in their mechanical response such as high work hardening rates or diminishing rate sensitivity of plastic deformation in CG FCC metals at low temperatures. During recovery annealing of cold worked structures dislocation based processes occur, reducing the defect densities as redundant dislocations annihilate and the substructure is reordered, followed by subgrain growth [9]. Consequently, such heat treatments lead to a softening of the material. However, recovery is not restricted to the cell or subgrains, since high angle grain boundaries (HAGB) can also act as sinks for lattice defects and may themselves reorder their structure during recovery treatments [11–13]. Decreasing the grain size not only increases the fraction of HAGBs, but also, once reaching the dimensions of typical dislocation substructures, dislocation-grain boundary interactions become dominant. In addition, the grain size is unfavorable for intragranular sources and dislocations are mostly emitted from grain boundaries [13]. Accordingly, for such fine grain sizes, the dominant and rate dependent processes not only during deformation, but also during annealing, are expected to change compared to CG samples.

Indeed, for nanostructured metals, a pronounced increase of hardness or strength can be obtained when using proper recovery heat treatments [1–4,14]. The hardening is attributed to a loss of dislocation debris due to accommodation of dislocations at the boundaries and the lack of intragranular sources, necessitating the activation of grain boundary sources. After annealing their activation is impeded, as rearrangement and equilibration processes of the boundary occurred [1–3,12]. The observation of segregation in some cases suggested that the hardening originates from strong interaction of dislocations with the segregated atoms [14–16]. Although such heat treatments can impressively alter the strength of nanostructured materials, their deformability is practically lost and deformation after the heat treatment will lead to strain softening [1] promoting early strain localization and failure.

The absence of frequent dislocation-dislocation interactions in nanostructured materials is also manifested in a change of the SRS and activation volume of plastic flow [5–7,17]. Compared to CG metals, in nanostructured samples, the SRS is reduced for bcc metals except for very fine grain sizes of ~ 10 nm, where again a slight increase was reported [5,18]. In contrast, a significant increase was measured for FCC materials, becoming more pronounced for smaller grain sizes [5,7]. Similar to the hardening phenomena, the increased rate sensitivity is generally related to the occurrence of dislocation grain boundary interactions [6,7,19,20]. Processes such as emission of (partial) dislocations [13,20,21], annihilation of lattice dislocations at grain boundaries [6] or, especially at low strain rates or applied stresses a shift from dislocation to GB mediated deformation processes such as grain boundary sliding or stress assisted boundary migration [22–25] were therefore suggested.

To date, most of the existing studies were performed at room temperature, while only some were carried out at slightly elevated temperatures, focusing mostly on nanocrystalline (NC) nickel [20,26–28]. A further increase of the rate sensitivity with testing temperature was measured. This increase of the SRS at elevated temperatures seems promising to enhance the formability of nanostructured materials that undergo anneal hardening, as enhanced strain rate sensitivities are known to stabilize deformation [29].
Therefore, the present study aims to identify the responsible processes leading to enhanced SRS in nanostructured metals, as this could offer the possibility to combine easy metal forming with attractive hardening mechanisms. Because both, anneal hardening and enhanced SRS, are thought to be related to dislocation-grain boundary interactions, materials were deliberately chosen such that interactions were already studied in detail on a CG scale [30]. Using the same materials with NC structures in the current study, we will show that the peak temperature for anneal hardening as well as the temperature leading to maximum SRS corresponds well with the reported average annihilation temperatures of dislocations at grain boundaries.

2) Experimental

Different FCC materials have been selected (316L steel, Ni 99.99 %, Ni4.5Al, Al1Mg, given compositions in wt-%) according to an earlier study on dislocation annihilation in HAGBs [30]. The high purity nickel was delivered from Good Fellow, while the 316L steel (Böhler grade A220) and the Al1Mg samples were purchased from standard suppliers. The Ni4.5Al samples were produced by arc melting. Buttons of about 30 g were remelted at least five times to ensure homogenous distribution of solute elements. All materials have been deformed by quasi-constrained high pressure torsion (HPT) at ambient temperature to produce nanostructured materials [31]. Disks of 8 mm diameter and 0.8 mm height were processed under an applied pressure of 7.8 GPa for 10 revolutions with a rotational speed of 0.2 rot/min, corresponding to a strain rate of $\dot{\varepsilon}$ = 0.05 s^{-1} at a radius of 3 mm. These strains are sufficiently large to obtain constant mechanical properties throughout the whole disk except for the very center part. All microstructural and mechanical investigations were conducted at a radius of 3 mm, yielding an equivalent von Mises strain of ε_{vM} = 136. The deformed samples were isothermally annealed for 30 min in selected temperature intervals and microhardness was measured on both, the as-deformed and annealed specimens in order to determine the onset temperatures for significant grain coarsening. These measurements were carried out along with quantitative grain size measurements of the as-deformed and additionally annealed microstructures. Apart from the NC 316L and Al1Mg samples, where microstructural evolution was already reported in previous studies [3,32,33], samples were analysed using electron backscatter diffraction (EBSD) data in radial direction of the HPT disk, acquired with a Zeiss LEO 1525 field emission gun scanning electron microscope (SEM). For clarification, the three principal axis of a HPT disk are shown in an inset in Fig. 1. Standard orientation imaging micrograph (OIM) software was applied to analyse the acquired data. A critical misorientation angle of 15 degrees was set for identification of a grain and only data points with a confidence index larger than 0.05 were taken into account to exclude unindexed pixels and to avoid possible errors introduced during data cleanup procedures. To determine possible phase decomposition upon deformation or annealing, conventional transmission electron microscopy (TEM) was applied on the alloyed samples. The specimens were prepared using standard methods followed by electrolytic thinning. The alloys were investigated in the as-deformed and annealed condition using an imaging-corrected JEOL JEM-2100 microscope operated at 200 keV.

Except for the pure Ni (99.99 %) samples, where SRS and activation volumes were already frequently reported for NC samples [7,17,20,27,28,34], both quantities were determined for the other three

materials at room temperature and in selected temperature regimes by nanoindentation strain rate jump tests. Indentation was carried out along the axial direction of the HPT disk. The surfaces were mechanically ground and polished, followed either by a mechano-chemical polishing step with colloidal silica (Ni4.5Al and Al1Mg), or by electro-polishing (316L steel) using a Struers electrolyte A2.

Local mechanical properties in terms of hardness and thermally activated deformation processes were investigated by means of nanoindentation using a platform Nanoindenter G200 (Keysight-tec, Santa Rosa, CA, USA). The system was equipped with a continuous stiffness measurement (CSM) unit, which superimposes a sinusoidal load signal in order to determine the contact stiffness, thus hardness and modulus, continuously over indentation depth. For elevated temperature testing a laser-heating stage (SurfaceTec, Hückelhoven, Germany) was used, where the tip and sample can be heated independently to adjust and stabilize the contact temperature and minimize thermal drift influences [35]. Moreover, a well-defined homogenous temperature distribution during the entire indentation process can be guaranteed. Additionally, during high temperature testing the entire system including sample tray and the Cu-cooling shield surrounding the heated indentation tip was actively water-cooled and the chamber temperature was kept close to 291 K. An inert gas flooded (forming gas – N_2 containing 5% H_2) environment was preserved by two individually controllable valves which regulate the gas flow around the sample tray and the heated tip. This allows an oven-like atmosphere, which reduces oxidation of the tested samples. After each experiment, the sample surface was inspected visually, but an oxide formation was not quantified. For all experiments three sided Berkovich pyramids were chosen, fabricated from diamond for room temperature testing (Synton-MDP, Nidau, Switzerland), while sapphire (Synton-MDP, Nidau, Switzerland together with Surface Tec, Hückelhoven, Germany) was selected for high temperature testing, since according to literature this minimized chemical interactions between tip and sample [36]. Frame stiffness as well as tip shape calibrations were performed on a regular base with the reference material fused silica according to the Oliver-Pharr method [37]. The initial allowable thermal drift for all temperatures was set to less than 0.1 nm/s and determined for each temperature before the start of every array, and additionally quantified after each indentation. Arrays of at least four indentations were performed at individually chosen temperatures within the heating and the cooling cycle, ranging between RT and maximum 723 K depending on the tested materials and expected properties (Ni4.5Al: 295, 323, 373, 423, 448, 473, 498, 523, 548, 573, 473 and 373 K; Al1Mg: 295, 323, 348, 373, 398, 423, 473, 523 and 423 K; 316L: 295, 373, 473, 523, 573, 623, 673 and 723 K).

All indentations were performed in a constant strain-rate controlled mode [38], where hardness and modulus were recorded continuously and averaged for a strain-rate of 0.05 s^{-1} between 1050 – 1450 nm indentation depth. Local strain-rate sensitivity and activation volume were calculated from nanoindentation strain-rate jump tests [39], where the applied strain rate was changed abruptly every 500 nm, starting at 0.05 s^{-1}, then dropping to 0.01 s^{-1}, followed by an increase to 0.05 s^{-1}, then dropping to 0.005 s^{-1}, and back to the initial strain rate of 0.05 s^{-1}. Thermally activated deformation processes were quantified instantaneously as described elsewhere [5,40] by calculating the SRS, m, and the apparent activation volume, V^*, according to Eq. (1), and Eq. (2)

$$m = \frac{\partial(\ln(H))}{\partial(\ln(\dot{\epsilon}))} \quad \text{Eq. (1)}$$

$$V^* = \frac{C^* * \sqrt{3} * k_B * T}{m * H} \quad \text{Eq. (2)}$$

where H denotes the hardness and $\dot{\epsilon}$ the strain rate, C^* being a constraint factor of 2.8, k_B the Boltzmann constant and T the absolute temperature.

3) Results

3.1) Mechanical properties and microstructural stability

Because both, the apparent activation volume, V^*, and the SRS, m, of plastic flow have been reported to be grain size dependent [5,7], knowledge of the thermal stability of the structures is essential to select a proper temperature range for the nanoindentation jump tests. To determine the maximum temperature, T_{max}, upon which the severely deformed structures remain stable, room temperature micro hardness measurements were carried out on the as-deformed as well as on isochronally annealed samples. Complementary, grain sizes of the samples were analysed based on electron microscopy investigations. Measurable onset of grain growth agrees with the hardness measurements. Evolution of room temperature hardness as a function of the annealing temperature (30 min annealing time) showed quite different trends for the investigated materials, see Fig. 1. The HPT deformed nickel and the Al1Mg samples showed a typical recovery behaviour of cold worked structures with slightly decreasing hardness up to a certain temperature T_{max}, before grain growth accompanied by a large drop in hardness occurred. The other investigated materials (Ni4.5Al, 316L) exhibited a quite pronounced increase of hardness with annealing temperature, peaking at T_{max}. For higher annealing temperatures, hardness decreased again along with slight grain coarsening, before at even higher temperatures pronounced grain growth accompanied by a severe drop in hardness occurred. Up to T_{max} the microstructures remained rather stable and even in the case of nickel and the aluminium alloy up to T_{max} no significant structural changes were observed, indicating that only defect annihilation was responsible for the hardness reduction. This temperature therefore separates pure recovery from the recrystallization and grain growth regime. However, T_{max} should only be considered as an approximate value for the onset of grain growth, as the intervals between the chosen annealing temperatures were rather wide. Although the temperature range for high temperature nanoindentation was restricted to the coarsening temperature, T_{max}, the slow growth rates of the Ni4.5Al and the Al1Mg alloys allowed to measure also at slightly higher temperatures, compare Fig. A1.

The maximum annealing temperature before grain growth occurred, T_{max}, the measured hardness values of the as-deformed state, H_{def}, and the maximum achievable hardness by a proper recovery annealing treatment, H_{max}, as well as the grain size, d, of all materials under investigation are summarized in Tab. 1. In addition, the average temperatures for dislocation annihilation in HAGBs of these materials as reported in [30] are listed in Tab. 1. Microtexture measurements based on the EBSD data showed for HPT deformation in the entire temperature range from room temperature up to T_{max} only the occurrence of ideal deformation texture components expected for simple shear [41]. This is exemplarily shown in Fig. 2 for the Ni4.5Al samples, where high intensities are present only close to the ideal positions indicated by black dots. Increasing the deformation temperature to 573 K only leads to a slight spread of the intensities. Texture measurements of the other samples (not shown) consistently revealed similar results. This emphasises that for all testing temperatures within this study during HPT dislocation based plasticity prevails. Furthermore, it is established that a HPT deformed structure in the saturation regime consist of about 70 - 80 % of HAGB which are random in nature, with no preferred misorientation angle or axis appearing, as previously reported for a variety of different materials [42–47].

Analysis of the Debye Scherrer rings of the as-deformed and annealed Al1Mg samples showed for both conditions only reflections of the FCC lattice, while for the Ni4.5Al samples an additional peak appeared in some areas, which could be identified to originate from nickel oxide (NiO), but formation of an intermetallic phase can be excluded in both cases, compare Fig. 3. Similarly, the NC 316L samples were

investigated previously, confirming the existence of a single FCC phase up to 823 K [3]. Thus, all samples used within this study can be treated as single phase FCC materials.

3.2) High temperature nanoindentation strain rate jump tests

As outlined above, nanoindentation strain rate jump tests were carried out on the various samples at different temperatures, starting at room temperature up to T_{max}, the thermal stability limit of the individual samples, except for the Al1Mg and Ni4.5Al samples, which were tested also at slightly higher temperatures. Because numerous data is already available on nanocrystalline and ultrafine-grained nickel (e.g. Refs. [7,17,20,27,28,34]), the pure nickel samples were excluded from this experimental effort. For each given temperature, the strain rates during indentation testing were changed repetitively in the range of 0.05 s^{-1} to 0.005 s^{-1}. The temperature dependency of the Young's modulus and hardness for all materials tested at a strain-rate of 0.05 s^{-1} are displayed in Fig. A2.
For all samples investigated, a similar behaviour was observed and the hardness response as a function of indentation depth, including multiple strain rate jumps, is shown exemplarily for the Ni4.5Al samples in Fig. 4. Moreover, the depth independent modulus data (small inlay) verifies the reliability of these indentations. Clearly, for all tested temperatures hardness is changing noticeable when the applied strain rate is altered. Hardness becomes smaller for reduced strain rates and larger for the higher strain rates tested. This indicates a positive SRS and no significant influence of the solute atoms on the plastic flow of the alloyed samples, at least in the investigated grain size and temperature range. Switching back to a previous strain rate leads to identical hardness levels as before, demonstrating that the tested structures are not only thermally but also mechanically stable during testing. From Fig. 4 it is evident that for higher testing temperatures the change in hardness due to a strain rate jump becomes more pronounced. Calculating the SRS, *m*, according to Eq. 1, and evaluating it as a function of temperature confirms this trend, see Fig. 5 and Tab. 2. For all tested materials, the SRS remains relatively low up to a certain temperature, although still an order of magnitude higher than for CG FCC metals. Above this temperature, the SRS increases noticeably with further temperature increase, see Fig. 5. At elevated testing temperatures especially the Ni4.5Al and the Al1Mg samples reach rather high SRS values of 0.1 and 0.15, respectively. Interestingly, the pronounced increase does not occur at similar homologous temperatures and is different for each material. While a strong increase of *m* could be measured for the Ni4.5Al samples starting already at 0.25 T_m, for the two other materials, Al1Mg and 316L, a pronounced increase of *m* does not occur below 0.35 T_m. Although the 316L samples could not be tested up to T_{max} due to the instrument limitation in testing temperature, also here an increase of *m* above a certain temperature is clearly visible. Thus, similar trends as for the other materials can be expected for higher testing temperatures. It is important to note that exposing the samples to higher testing temperatures does not alter the SRS values when testing back at lower temperatures, exemplarily shown for the Ni4.5Al samples in Fig. 5. Clearly, the measurements performed during the heating cycle perfectly match with the ones obtained during cooling at the same testing temperature. This can be attributed to the negligible growth of Ni4.5Al grains, although T_{max} was exceeded. However, this does not hold true in case distinct coarsening occurred during the high temperature tests, as for the Al1Mg samples that were tested well above their stability limit (~ 400 K). Strain rate jump tests on those samples performed during the cooling cycles at somewhat lower temperatures showed even a negative SRS (m= -0.003), as expected for CG as well as UFG AlMg alloys in a suited temperature range [40,48]. Interestingly, although the grains already coarsened to some extent as T_{max} was exceeded for Ni4.5Al and Al1Mg during the heating cycle, the SRS did not drop as would be expected, see Fig. 5. This behaviour could be related to the persisting high grain boundary density present

for both materials (Fig. A1), as it was previously shown that for significant grain growth, a pronounced drop of the SRS occurs [49,50].

Fig. 6 summarizes the calculated values of the apparent activation volume V^* for all materials as a function of testing temperature. The calculated values for V^* are on the order of several tens of b^3 for all materials and about one to two orders of magnitude smaller than observed in CG FCC metals, see Fig. 6 and Tab. 2. Measured V^* values of the Al1Mg alloy at ambient temperature are significantly larger than those of the others, which can be related to the relatively low hardness values of this alloy compared to the other samples tested, compare Eq. (2) and Tab. 1. Similar to the SRS, the values measured during the cooling cycle showed no significant difference compared to the ones obtained during the heating cycle, see Fig. 6. While the overall trends for the SRS are similar for all tested materials, this does not appear on first view for the activation volumes. Except for Al1Mg, the other two materials showed increasing or relatively constant V^* values at moderate testing temperatures ranging from 10 to $30 \cdot b^3$, which are decreasing again at higher temperatures. Different, for the Al1Mg samples, V^* continuously decreased with an increase of testing temperature until reaching relatively constant values of about 10 b^3. However, these are tested already above $0.30 \cdot T_m$, where also for the other samples a decrease of V^* was observed. Taking a closer look on the parameters influencing V^* (Eq. 2) and their evolution with temperature (Fig. 4, Fig. A1) it becomes clear, that the pronounced reduction of V^* is for all materials occurring at the temperature where also the rate sensitivity, m, starts to increase markedly. As V^* serves as a fingerprint of the underlying deformation mechanisms and processes, this suggests that the processes leading to enhanced SRS also provoke the reduction of the activation volume.

4) Discussion

Nanoindentation revealed distinct differences of the various nanostructured FCC metals compared to their CG counterparts. For all materials consistent trends were measured and already at room temperature enhanced SRS values of about 0.02 were determined (Tab. 2). As shown in Fig. 5, SRS values increase further up to 0.1 and 0.15 above certain testing temperatures for the Ni4.5Al and Al1Mg samples, respectively. On the other hand, compared to CG materials significantly reduced apparent activation volumes of $10 – 60 \cdot b^3$ were determined. These results are consistent with earlier findings on the SRS and activation volume of NC or ultrafine-grained (UFG) materials, see for example [5–7,20,28]. The increased SRS and decreased activation volumes compared to CG metals are generally explained by a change in the underlying rate controlling processes, when the grain size is reduced to the submicrometer regime. Yet, still discrepancies about the dominant and rate controlling processes causing the investigated effects are reported in literature [6,7,20,21]. However, as the average annihilation temperatures of lattice dislocations in HAGBs [30] match with those where maximum SRS values and onset of grain growth occurred in the severely deformed materials (compare Tab. 1), in the remainder we will discuss how accommodation of dislocations at grain boundaries can serve as basic mechanism to explain the measured trends in SRS, and how it can be linked with the onset of grain coarsening.

To understand the reasons that provoke the enhanced SRS of the NC materials, let us first consider the underlying processes at the mesoscale. As indicated by the deformation textures in Fig. 2, for the grain sizes and temperature intervals tested here plasticity is still dislocation based. Therefore, any change in the rate controlling processes cannot be explained by a change of the deformation mechanisms, but has to be related to differences in dislocation slip in these confined volumes. If during plastic deformation lattice dislocations enter a grain boundary, so called extrinsic grain boundary dislocations (EGBDs) are formed. The term extrinsic refers to the fact that they are not part of the equilibrium grain boundary

structure [51,52]. These intergranular dislocations are accommodated either by decomposition into ones having smaller burger vectors, in case of infinitesimal small ones also referred to as dislocation spreading [51,52]. Anyway, these processes leading to a relaxation of the grain boundaries and reduction of their energy, require temperatures high enough to enable local rearrangements or mobility of these defects within the boundary. Therefore, only above sufficient temperatures thermally induced intergranular stress relaxation can occur. As mentioned, the obtained SRS values peaked close to T_{max} (Tab. 2), agreeing well with the average annihilation temperature of lattice dislocations, compare [30]. Based on the considerations above, this is not surprising. Above a certain temperature, impinging lattice dislocations can be thermally accommodated and their stress fields decay with time. Therefore, testing a material at sufficiently high temperatures and low strain rates, the annihilation process of the dislocation at the grain boundary take place before a subsequent dislocation enters the boundary. In this case, the remaining stress field of the lattice dislocations is already relaxed, causing reduced interaction. On the other hand, for high strain rates, the accommodation may not be complete and subsequent dislocations interact with the remaining stress fields, leading to enhanced stresses required for plastic deformation. In principle, once a material is tested at temperatures where dislocations can thermally annihilate at grain boundaries, no SRS should be measured at all, as no stress field will remain to interact with subsequent dislocations. However, transmission electron microscopy (TEM) studies on intergranular dislocation absorption indicate that this is not a spontaneous process, rather the stress contrast of the dislocations vanishes with time [30,53]. Nevertheless, absorption kinetics might be enhanced above some temperature to a rate comparable to that of the flux of incoming dislocations, resulting in a decrease of the SRS. To evaluate if such temperatures are potentially reached in the present experiments, we can estimate the underlying time scales for deformation and intergranular stress relaxation. As an example we consider the Ni4.5Al samples with an average grain size of d = 120 nm. Taking into account the equivalent strain caused by the Berkovich indenter of ε = 0.08 and the burgers vector b = 0.25 nm, the necessary number of dislocations per grain, N_{dis}, to realize this strain can be estimated to be $N_{dis} = \varepsilon d/b$, yielding values of about 40. Considering the lowest strain rates applied within the experiments, $\dot{\varepsilon}$ = 0.005 s^{-1}, time scales of about a second between individual dislocations entering a grain boundary can be assumed. On the other hand, the relaxation time, τ, of an array of random EGBDs at a given temperature T, can be calculated according to Eq. 4, [52,54]

$$\tau = A \frac{k_B T s^3}{G \Omega D_{GB} \delta} \qquad \text{Eq. (3)}$$

where A denotes a constant (for severely deformed materials found to be 1/200 [54,55]), k_B the Boltzmann constant, s the spreading distance, G the shear modulus, Ω the atomic volume, D_{GB} the grain boundary self-diffusion coefficient and δ the grain boundary width (usually taken as 0.5 nm). In case the spreading distance equals the grain size, the boundary can be considered to be completely relaxed. Thus, the appropriate value of the relaxation time can be considered as the required time scale to remove remaining stress fields from inserted dislocations. Again, the Ni4.5Al samples are considered at maximum testing temperature (573 K). The shear modulus (64 GPa) is taken from the nanoindentation results, the boundary width as 0.5 nm and the atomic volume for nickel as 10.9 Å³ [55]. Because reliable grain boundary diffusivities for Ni4.5Al are not available for the desired temperature range, the ones obtained on severely deformed nickel with low purity (99.6 %) will be used as an approximation (D_{GB} = 1.8*10^-5 *exp(-

162000/RT)) [56]. Accordingly, relaxation times of about 6500 s are derived, being orders of magnitude larger than the relevant time scales for deformation imposed by the nanoindenter.

Therefore, as the temperatures where maximum SRS values were measured agree with the ones observed for annihilation of lattice dislocations in the same materials, one might conceive that the mechanism responsible for the increase of SRS at elevated temperatures is thermally activated accommodation of lattice dislocations within the grain boundaries. Reducing the testing temperature not only causes an increase of the relaxation time, but also that such processes may not occur on all types of boundaries, reflected in reduced SRS values measured. Depending on the exact nature of the boundary, different annihilation temperatures have been reported, being significantly higher for special boundaries such as low sigma ones [30,52]. Below a certain temperature, thermally activated accommodation of dislocations is inhibited, but similar accommodation processes can be considered based on a mechanical driving force. In that case, the applied strain rate does not influence the accommodation kinetics significantly, resulting in the observed low rate dependency of mechanical properties, becoming almost independent of testing temperature. Such mechanical incorporation of dislocations into GBs was also experimentally observed and it was found that small pile-ups or stress fields from subsequent dislocations can accelerate this mechanically driven accommodation process [53]. For sufficiently low testing temperatures, this process can be considered to occur purely mechanically driven and no rate dependency is to be expected. Such change from a thermally activated to a mechanical driven accommodation of dislocations into the boundary is comparable to observations of boundary migration in nanostructured materials, which progressively changes from a thermally to a mainly mechanically driven one at low temperatures [57,58]. The transition from thermally to mechanically activated accommodation can be expected to be also reflected in different apparent activation energies, Q, of the underlying processes. For mainly mechanical activation, as previously suggested for migration of boundaries in nanostructured metals [57,58], significantly reduced Q values can be assumed. The apparent activation energy, Q, can be evaluated from indentation data using the modulus-compensated hot hardness analysis [59]. Accordingly, Q is related to the hardness H, and the Young's modulus E, by Eq. (3).

$$\frac{H}{E} = G' * \exp^{(\frac{Q}{nRT})} = G' * \exp^{(\frac{Qm}{RT})} \quad \text{Eq. (4)}$$

In Eq. 3, G' is a pre-exponential factor, R the gas constant, T the absolute temperature and n the stress exponent, related to the rate sensitivity m via n = 1/m. Fig. 7 shows the ln(H/E) over 1/T plots for all investigated materials. Within certain temperature intervals, the data can be well described by a linear fit, except for the data of the NC 316L steel at low temperatures. From the slope of these linear fits the apparent activation energy Q can be deduced. As the SRS m itself changes with temperature (Fig. 5), for the calculation of the activation energy Q, the average value of m in the two distinct regimes was used to determine Q, see Fig. 7. Obviously, depending on the testing temperature, two distinct regimes with different activation energies can be distinguished, with a crossover occurring at a critical temperature T_c. For comparison, this temperature T_c is also indicated for each material in Fig. 5 and Fig. 6 as well. Doing so, for the Ni4.5Al samples, at low testing temperatures a relatively low activation energy of Q = 27.4 kJ/mol is calculated, while the one at elevated testing temperatures yields higher values of Q = 120.1 kJ/mol. Similarly, for the other materials tested, two distinct regimes are identified, and the calculated activation energies for both regimes are summarized in Tab. 2. In the high temperature regime (larger Q

values) one would expect activation energies similar to those for boundary diffusion, as the dislocation absorption requires rearrangements within the boundary, compare Eq. (4). Grain boundary diffusion data for Ni4.5Al and 316L are not accessible; however, data for AlMg alloys with slightly higher Mg concentration is available. Therefore, focusing on the Al1Mg samples, the activation energy of the rate controlling processes at higher testing temperatures (Q = 87.3 kJ/mol) is in good agreement with literature data for grain boundary diffusion in AlMg alloys of Q ~ 90 kJ/mol [60,61]. Similarly, the calculated activation energies for the Ni4.5Al samples in the high temperature regime are in the range for those obtained from grain boundary diffusion measurements on nickel [56]. This provides additional evidence for thermally activated dislocation accommodation being the rate controlling process responsible for enhanced SRS values, especially at elevated temperatures. Therefore, T_c separates to our notion the mechanically dominated regime from that where accommodation of dislocations at grain boundaries starts to become possible. Indeed, around T_c, SRS starts to become temperature sensitive. As mentioned before, at this temperature at certain boundaries thermally induced processes become dominant, whereby the exact temperature will differ from boundary to boundary. Pumphrey and Gleiter reported for all materials an annihilation temperature spectrum of about ± 50 K around the average values [30]. This temperature spectrum is in line with the difference between T_c and T_{max} of about 50 – 100 K for the aluminium and nickel alloy tested. However, for the 316 L steel this difference is notably larger. The reason for this could be related to the difference in the microstructure between the samples. In case of the 316 L steel, many nanocrystallites are further subdivided by twins [32]. Accommodation of dislocations at twin boundaries requires significantly higher temperatures, and instead of a spreading climb within the boundary plane is more likely to occur [30,52].Therefore, this significant difference between the involved boundaries likely causes the enhanced temperature window between T_c and $T_{\underline{max}}$ in case of the NC 316L steel.

Taking a closer look at the trends for the apparent activation volumes V^*, which serves as fingerprint of the underlying processes and deformation mechanisms, supports this conclusion. For all materials, V^* evidently starts to decrease to lower values at the temperature where the SRS starts to increase significantly. This reduction cannot be explained by precipitation of intermetallic particles at the grain boundaries that could limit the moving distance of a dislocation between pinning points, see Fig. 3. Rather, we consider this reduction as a signature of the rearrangements or defect movement occurring within the grain boundary necessitating diffusion based processes. While such processes are expected to result in single digit activation volumes, dislocation based processes in nanostructures manifest in values of several tens of b^3. As dislocation based plasticity prevails for all testing temperatures (Fig. 2), the reduction of V^* may be a consequence of measuring an effective value of both processes, emission and propagation of dislocations through the grain in conjunction with the thermally induced rearrangements after absorption. It is interesting to note that measurements taken during the cooling cycles on the Ni4.5Al samples gave identical values for m and V^* as obtained during the heating cycle, see Fig. 5 and 6. This confirms that the microstructures were stable. Furthermore, it indicates that segregation and relaxation of grain boundaries, possibly occurring at elevated testing temperatures, does not influence the mechanical properties when testing them again at lower temperatures, at least for the accessible strains and strain rates applied during indentation. Similar results have been obtained on NC Ni-W for grain sizes larger than 10 nm [2]. If pinning or strong interaction of dislocations with boundary ledges or impurities would play a distinct role as suggested for instance in [15,62], different values should be measured during the cooling cycle. However, to clarify such influence on the dislocation nucleation from boundaries, similar measurements with an

indenter tip having a larger opening angle, realizing reduced equivalent strains, or testing with a spherical indenter would be necessary.

As mentioned before, the thermal stability limit also showed good agreement with the reported average annihilation temperatures of lattice dislocations in random HAGBs, compare Tab. 1 and [30]. For the materials undergoing anneal hardening, the maximum hardness of the nanostructures could be obtained by annealing treatments at or close to these temperatures, see Tab. 1 and Fig. 1. Again, the excellent agreement between these temperatures can be understood considering the processes at the mesoscale. Grain coarsening necessitates the movement of grain boundaries, which occurs by the motion of boundary steps, either thermally induced or due to the interaction with external stress fields. Indeed, boundary migration in submicron sized metals caused by the movement of disconnections (i.e. steps associated with a dislocation) under applied temperature and mechanical load has been investigated recently [63–65]. Such disconnections can also be generated by absorption of lattice dislocations into the grain boundary [64]. Therefore, it is not surprising that at temperatures where accommodation can occur frequently, boundary migration will take place as well. This is also in agreement with recent observations where structural coarsening in severely deformed metals was found to initiate by motion of triple junctions which can be easily pinned by lattice defects such as dislocations or substructures within the grain [66]. Accordingly, if lattice dislocations can be accommodated at boundaries at a given temperature, the movement of the junctions is facilitated and coarsening proceeds. We can therefore understand the processes occurring at the peak temperature as a competition between grain growth and recovery, involving at least for submicron grain sizes still a reduction of the intragranular dislocation content and relaxation of boundaries, as suggested earlier [1]. The fact that anneal hardening is occurring already at temperatures below T_{max} (see Fig. 1) is not contradicting the explanation above, as accommodation of dislocations is not occurring at a specific temperature for a given material, but in a certain temperature spectrum, depending on the exact character of the boundary such as misorientation angle, excess volume and local chemistry [30,67,68]. For this reason the good agreement between the average temperatures observed in the present work and those reported in [30] are not surprising, as HPT and related processes of severe plastic deformation are known to produce random boundary structures in the saturation regime [42–47].

Another astonishing finding was that the thermal stability, or the temperatures leading to the peak hardness, of various nickel samples reported in literature [7,62,69–72] was close to 473 K, which was also the annihilation temperature in Ref. [30]. As Pumphrey and Gleiter reported in their study, grain boundary migration did in any case occur after or during the dislocation spreading process, but never prior to it [30]. This seems at first glance not surprising as both processes, accommodation and migration, necessitate rearrangements in the boundary region. However, the referenced nickel samples had quite different grain sizes, ranging from 30 nm up to 200 - 300 nm. Based on Eq. (3), which provides an estimate of the relaxation time, one would expect a pronounced difference of the relaxation times for samples having different grain sizes. In fact, the differences in grain size of the compared samples (30 nm versus 200 nm, respectively) should reduce the relaxation time and so presumably the migration/growth kinetics by a factor of 300. However, this would only be the case if all other parameter could be kept constant. In case of the referenced nickel samples this will not be the case, as for synthesis of the finest grain sizes always a certain amount of impurity atoms is necessary. As mentioned earlier, the activation energy for boundary diffusivity is quite sensitive to the purity level [56]. Due to the exponential dependency of the boundary diffusivity on the activation energy, the difference induced by the grain size can be easily surpassed,

rendering it the more important parameter in Eq. (3). The correlation of extrinsic grain boundary dislocation stability with boundary migration and its strong dependency on the boundary diffusivity may provide, apart from the well-established kinetic and thermodynamic approaches [73–75], a different view on the thermal stability of nanostructures.

5) Summary and conclusions

In the present study the annealing response, strain rate sensitivity and apparent activation volume of several nanostructured FCC materials were investigated by high temperature nanoindentation jump tests. The materials were chosen with respect to a previous study focussing on annihilation of lattice dislocations in high angle boundaries for a CG microstructure. The results showed excellent agreement between these bulk annihilation temperatures and the thermal stability of the tested nanomaterials. Samples that undergo anneal hardening reach a peak hardness close to these temperatures. Similarly, the strain rate sensitivity is increasing with temperature and peaks at these critical temperatures. The results suggest that the enhanced strain rate sensitivity at elevated temperatures originates from thermally activated annihilation of lattice dislocations at high angle grain boundaries. This is supported by the measured activation energies of the responsible processes which are in the range expected for grain boundary diffusion. In contrast, at low temperatures the accommodation process is mainly mechanically driven. Although the rate sensitivity generally increased for all materials, quite different absolute values among the individual materials were measured. As dislocation accommodation is closely related to interfacial diffusivity, future work should be devoted to understand which interface design improves these properties and how it can be controlled, as this would pave the way for enhanced formability of nanostructured materials.

Acknowledgements

Financial support by the European Research Council under ERC Grant Agreements No. 340185 USMS and No. 771146 TOUGHIT, by the Austrian Science Foundation (FWF) under project P25325-N20 and by the Austrian Federal Government (837900) within the framework of the COMET Funding Programme (MPPE, project A7.19) is gratefully acknowledged. OR would like to thank Dr. Jean-Philippe Couzinie (Université Paris Est) and Prof. Louisette Priester (Université Paris Sud) for valuable and stimulating discussions regarding dislocation-grain boundary interactions. J.H. Li acknowledges National Key Research and Development Program of China [2016YFE0115300]; Major International (Regional) Joint Research Project [51420105005]; and Overseas, Hong Kong, Macao Scholars Cooperative Research Fund [51728101].

Appendix

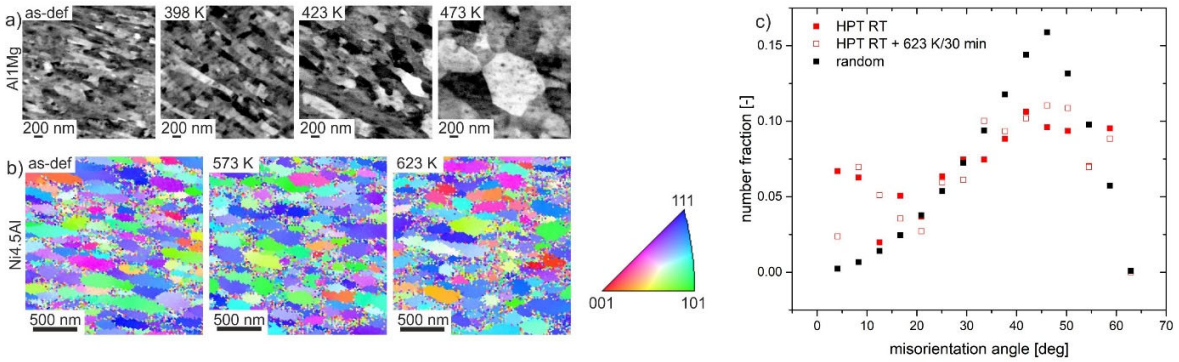

Fig. A1) a,b) Representative micrographs of the investigated Al1Mg and Ni4.5Al alloys in the as-deformed state and after various annealing conditions. Grain growth occurs rather slow for both alloys, especially for the Ni4.5Al samples. c) Misorientation distribution of the Ni4.5Al alloy in the as-deformed and annealed condition confirming that the majority of the grain boundaries is of high angle type being almost random in nature.

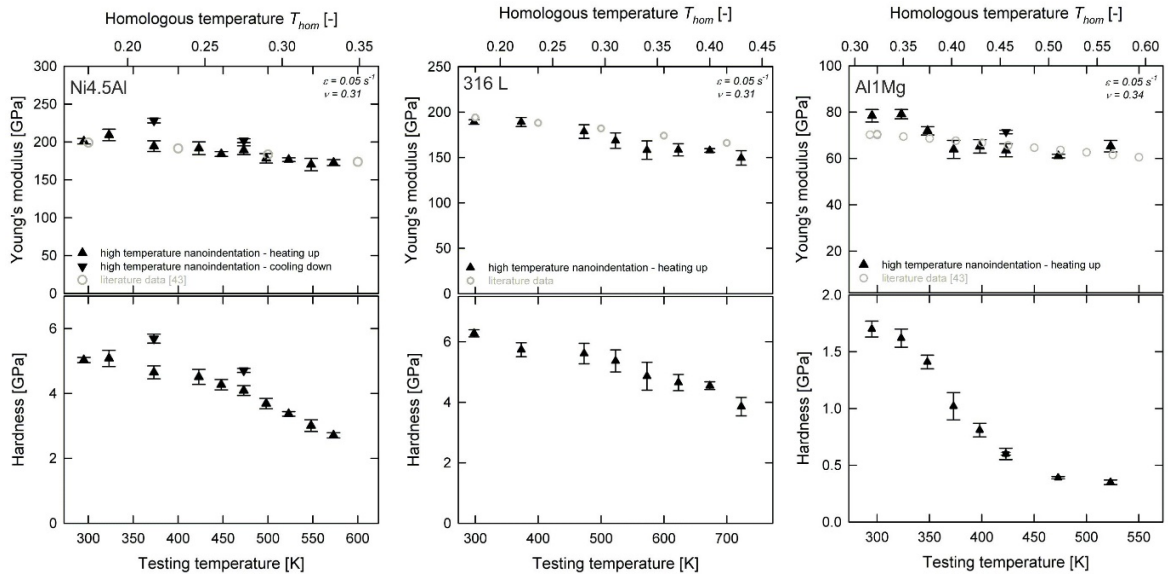

Fig. A2) Young's Modulus and Hardness of the various materials as a function of the testing temperature. For the Ni4.5Al samples measurements from the heating and cooling cycle are displayed.

List of tables

Table 1) Overview of the mechanical properties, grain sizes and critical annealing temperatures of the various samples investigated. H_{def}, denotes the hardness of the as-deformed samples, H_{max}, the maximum hardness achievable after a 30 min recovery annealing treatment with the standard deviation giving the error bar. d, denotes the average equivalent grain size after HPT deformation, and T_{max}, the maximum temperature before significant grain growth occurs. $T_{annihilation}$ denotes the average temperature for dislocation annihilation in high angle grain boundaries as reported in [30]. Please note that the compositions used in [30] slightly differ from those used in the present study.

Material	H_{def} [GPa]	H_{max} [GPa]	d [nm]	T_{max} [K]	$T_{annihilation}$ [K] [30]
Al1Mg	1.40 ± 0.02	-	~ 200 [33]	398 K ± 12.5 K	~ 413 K (Al0.9Mg)
Ni (99.99%)	3.19 ± 0.01	-	239 ±137	423 K ± 25 K	~ 493 K
Ni4.5Al	4.19 ± 0.02	4.44 ± 0.01	120 ± 66	523 K ± 25 K	~ 573 K (Ni5Al)
316L	5.01 ± 0.02	5.94 ± 0.02	~ 60 [32]	823 K ± 12.5 K	~ 773 K (Fe25Ni20Cr)

Table 2) Strain rate sensitivity, m, and apparent activation volume, V^*, measured by nanoindentation at room temperature (m_{RT}, V^*_{RT}) and elevated temperature (m_{max}, V^*_{HT}) where maximum values of m have been determined. Values of m and V^* for Ni are taken from Refs. [7,20,27,28]. The apparent activation energy, Q, was calculated based on Ref. [59] for the two clearly distinguishable regimes at lower and higher temperatures (Fig. 7).

Material	m_{RT} [-]	m_{max} [-]	V^*_{RT} [b³]	V^*_{HT} [b³]	$Q_{T\,low}$ [kJ/mol]	$Q_{T\,high}$ [kJ/mol]
Al1Mg	0.009 ± 0.001	0.15 ± 0.06 (423 K)	57.1 ± 7.5	13.7 ± 0.3	72.6 ± 0	87.3 ± 5.4
Ni	0.015 - 0.04	0.12 (473 K)	15 - 30			
Ni4.5Al	0.014 ± 0.001	0.096 ± 0.005 (573 K)	18.3 ± 1.0	9.0 ± 0.8	27.4 ± 3.0	120.1 ± 15.2
316L	0.017 ± 0.0002	0.041 ± 0.003 (723 K)	11.6 ± 0.1	17.1 ± 0.5	12.2 ± 16.9	80.6 ± 7.0

List of Figures

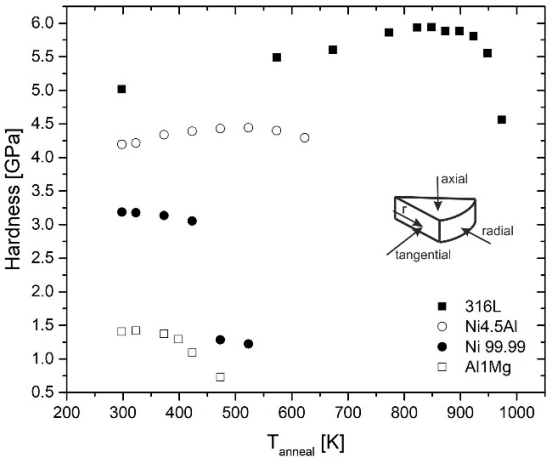

Fig. 1) Evolution of room temperature microhardness of the investigated samples as a function of the annealing temperature. In all cases, the duration of the heat treatments was fixed to 30 minutes. The inset image indicates the three principle axis of a HPT disk.

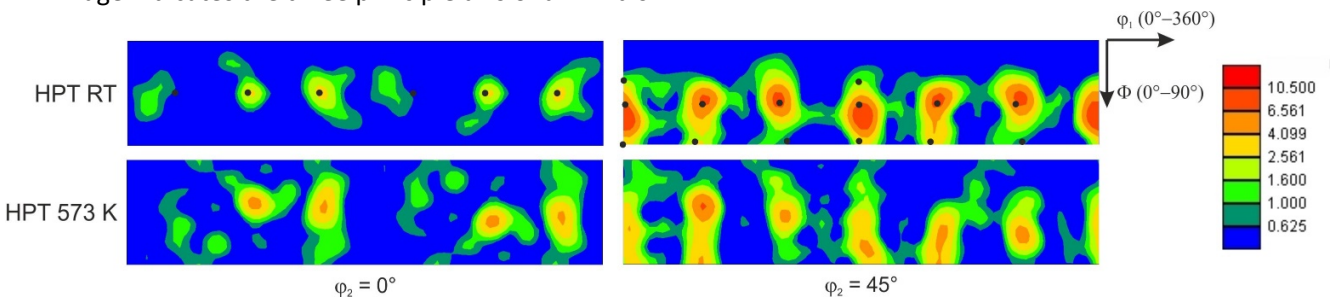

Fig. 2) Orientation distribution function (ODF) sections of a Ni4.5Al sample deformed by HPT at different temperatures. The appearance of expected deformation texture components provides evidence that dislocation based plasticity prevails for all test temperatures. Black data points indicate the position of ideal shear texture components [41].

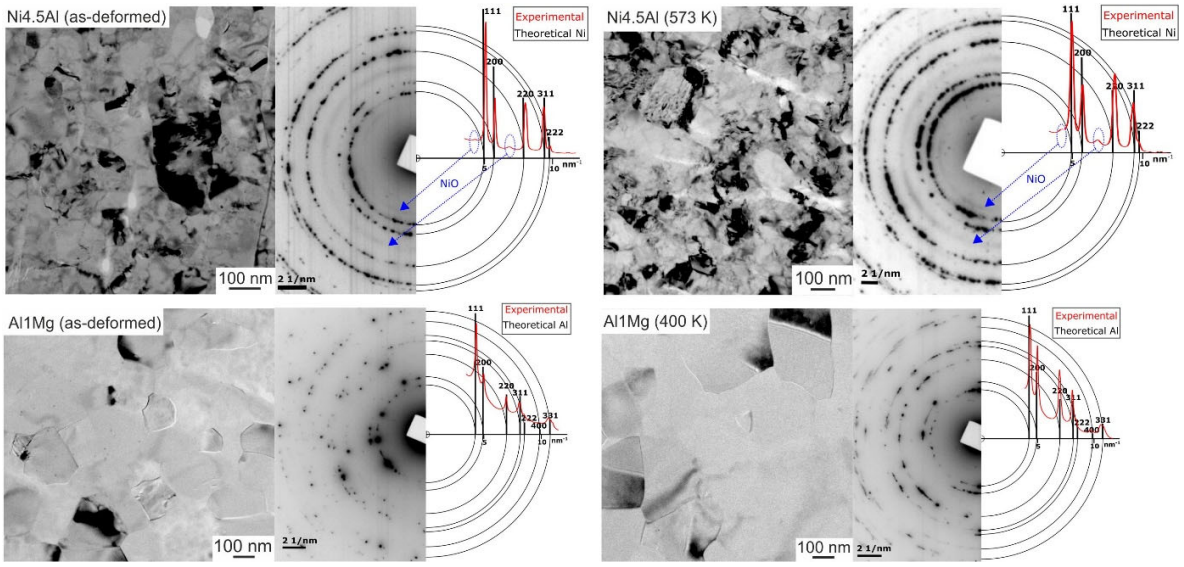

Fig. 3) Representative bright field images and experimental Debye Scherrer rings compared to the theoretical ones of the Ni4.5Al and the Al1Mg samples after HPT and additional annealing treatments. Except for the NiO peaks (highlighted in blue), no additional reflections except for the expected FCC ones were observed.

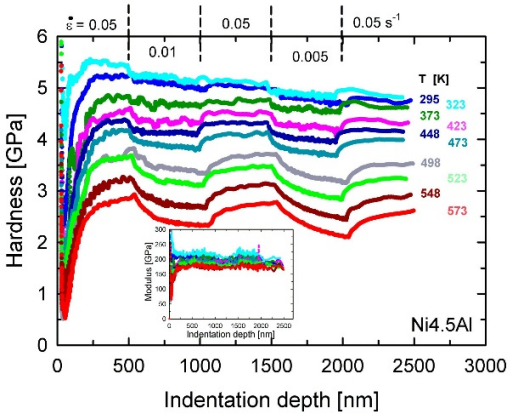

Fig. 4) Change of hardness as a function of the indentation depth over which multiple strain rate jumps have been performed exemplarily shown for the Ni4.5Al samples at various temperatures. A positive strain rate sensitivity is evident, being more pronounced for higher testing temperatures.

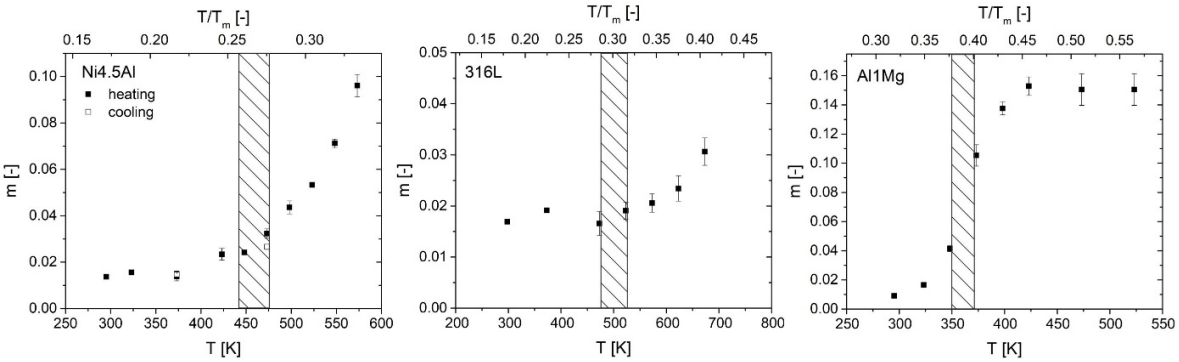

Fig. 5) Strain rate sensitivity, *m*, as a function of test temperature showing a common trend for all tested materials. At low temperatures *m* remains relatively constant, but increases significantly after exceeding a specific temperature. The Ni4.5Al samples were also tested during the cooling cycle and exhibited identical values compared to the heating cycle. The shaded area indicates the critical temperature range where the activation energy of the underlying processes changes, as detailed later.

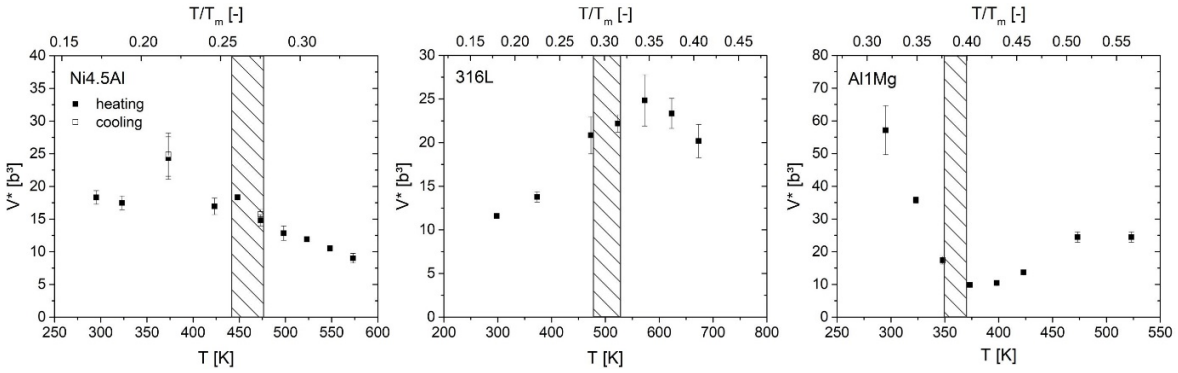

Fig. 6) Apparent activation volume, *V**, as a function of the testing temperature for the investigated materials. The critical temperature range where the activation energy of the underlying processes changes is highlighted.

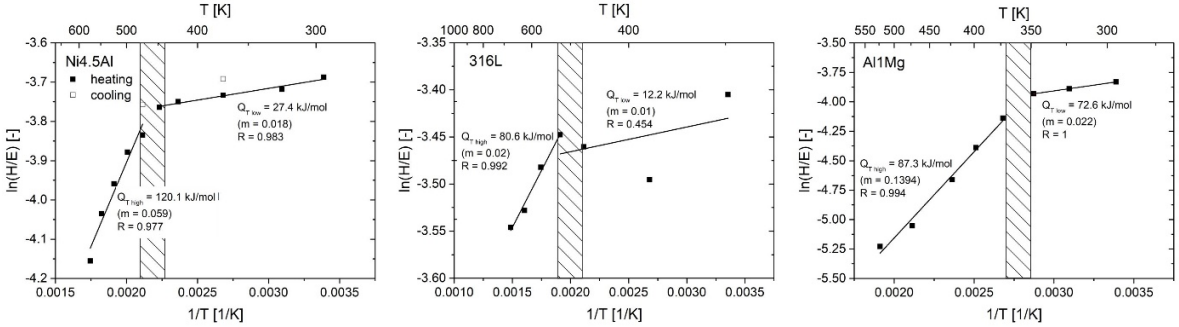

Fig. 7) Modulus compensated hardness as a function of the inverse temperature for all materials. Two regimes with different activation energies can be identified, with a crossover from mainly mechanically to thermally induced dislocation accommodation at a critical temperature T_c.

References

[1] X. Huang, Hardening by Annealing and Softening by Deformation in Nanostructured Metals, Science (80-.). 312 (2006) 249–251. doi:10.1126/science.1124268.

[2] T.J. Rupert, J.R. Trelewicz, C.A. Schuh, Grain boundary relaxation strengthening of nanocrystalline Ni–W alloys, J. Mater. Res. 27 (2012) 1285–1294. doi:10.1557/jmr.2012.55.

[3] O. Renk, A. Hohenwarter, K. Eder, K.S. Kormout, J.M. Cairney, R. Pippan, Increasing the strength of nanocrystalline steels by annealing: Is segregation necessary?, Scr. Mater. 95 (2015). doi:10.1016/j.scriptamat.2014.09.023.

[4] J. Hu, Y.N. Shi, X. Sauvage, G. Sha, K. Lu, Grain boundary stability governs hardening and softening in extremely fine nanograined metals, Science (80-.). 355 (2017) 1292–1296. doi:10.1126/science.aal5166.

[5] Q. Wei, S. Cheng, K.T. Ramesh, E. Ma, Effect of nanocrystalline and ultrafine grain sizes on the strain rate sensitivity and activation volume: Fcc versus bcc metals, Mater. Sci. Eng. A. 381 (2004) 71–79. doi:10.1016/j.msea.2004.03.064.

[6] H.W. Höppel, J. May, P. Eisenlohr, M. Göken, Strain-rate sensitivity of ultrafine-grained materials, Zeitschrift Für Met. Res. Adv. Tech. 96 (2005) 566–571. doi:10.1016/j.scriptamat.2005.03.043.

[7] H. Vehoff, D. Lemaire, K. Schüler, T. Waschkies, B. Yang, The effect of grain size on strain rate sensitivity and activation volume - From nano to ufg nickel, in: Int. J. Mater. Res., 2007: pp. 259–268. doi:10.3139/146.101464.

[8] N. Hansen, R.F. Mehl, A. Medalist, New discoveries in deformed metals, Metall. Mater. Trans. A. 32 (2001) 2917–2935. doi:10.1007/s11661-001-0167-x.

[9] A. Rollett, F. Humphreys, G.S. Rohrer, M. Hatherly, Recrystallization and Related Annealing Phenomena: Second Edition, 2004. doi:10.1016/B978-0-08-044164-1.X5000-2.

[10] M.R. Staker, D.L. Holt, The dislocation cell size and dislocation density in copper deformed at temperatures between 25 and 700°C, Acta Metall. 20 (1972) 569–579. doi:10.1016/0001-6160(72)90012-0.

[11] M.W. Grabski, R. Korski, Grain boundaries as sinks for dislocations, Philos. Mag. 22 (1970) 707–715. doi:10.1080/14786437008220941.

[12] A. Hasnaoui, H. Van Swygenhoven, P.M. Derlet, On non-equilibrium grain boundaries and their effect on thermal and mechanical behaviour: A molecular dynamics computer simulation, Acta Mater. 50 (2002) 3927–3939. doi:10.1016/S1359-6454(02)00195-7.

[13] H. Van Swygenhoven, P.M. Derlet, A.G. Frøseth, Nucleation and propagation of dislocations in nanocrystalline fcc metals, Acta Mater. 54 (2006) 1975–1983. doi:10.1016/j.actamat.2005.12.026.

[14] T.D. Shen, R.B. Schwarz, S. Feng, J.G. Swadener, J.Y. Huang, M. Tang, J. Zhang, S.C. Vogel, Y. Zhao, Effect of solute segregation on the strength of nanocrystalline alloys: Inverse Hall-Petch relation, Acta Mater. 55 (2007) 5007–5013. doi:10.1016/j.actamat.2007.05.018.

[15] R.Z. Valiev, N.A. Enikeev, M.Y. Murashkin, V.U. Kazykhanov, X. Sauvage, On the origin of the extremely high strength of ultrafine-grained Al alloys produced by severe plastic deformation, Scr. Mater. 63 (2010) 949–952. doi:10.1016/j.scriptamat.2010.07.014.

[16] M.M. Abramova, N.A. Enikeev, R.Z. Valiev, A. Etienne, B. Radiguet, Y. Ivanisenko, X. Sauvage, Grain boundary segregation induced strengthening of an ultrafine-grained austenitic stainless steel, Mater. Lett. 136 (2014) 349–352. doi:10.1016/j.matlet.2014.07.188.

[17] R. Schwaiger, B. Moser, M. Dao, N. Chollacoop, S. Suresh, Some critical experiments on the strain-rate sensitivity of nanocrystalline nickel, Acta Mater. 51 (2003) 5159–5172. doi:10.1016/S1359-6454(03)00365-3.

[18] D. Jang, M. Atzmon, Grain-size dependence of plastic deformation in nanocrystalline Fe, J. Appl. Phys. 93 (2003) 9282–9286. doi:10.1063/1.1569035.

[19] Y.M. Wang, E. Ma, Strain hardening, strain rate sensitivity, and ductility of nanostructured metals, Mater. Sci. Eng. A. 375–377 (2004) 46–52. doi:10.1016/j.msea.2003.10.214.

[20] Y.M. Wang, A. V. Hamza, E. Ma, Temperature-dependent strain rate sensitivity and activation volume of nanocrystalline Ni, Acta Mater. 54 (2006) 2715–2726. doi:10.1016/j.actamat.2006.02.013.

[21] J. Lian, C. Gu, Q. Jiang, Z. Jiang, Strain rate sensitivity of face-centered-cubic nanocrystalline materials based on dislocation deformation, J. Appl. Phys. 99 (2006). doi:10.1063/1.2186981.

[22] D.S. Gianola, D.H. Warner, J.F. Molinari, K.J. Hemker, Increased strain rate sensitivity due to stress-coupled grain growth in nanocrystalline Al, Scr. Mater. 55 (2006) 649–652.

doi:10.1016/j.scriptamat.2006.06.002.

[23] Y. Wei, A.F. Bower, H. Gao, Enhanced strain-rate sensitivity in fcc nanocrystals due to grain-boundary diffusion and sliding, Acta Mater. 56 (2008) 1741–1752. doi:10.1016/j.actamat.2007.12.028.

[24] L. Wang, B.C. Prorok, Characterization of the strain rate dependent behavior of nanocrystalline gold films, J. Mater. Res. 23 (2008) 55–65. doi:10.1557/jmr.2008.0032.

[25] M.R. He, S.K. Samudrala, G. Kim, P.J. Felfer, A.J. Breen, J.M. Cairney, D.S. Gianola, Linking stress-driven microstructural evolution in nanocrystalline aluminium with grain boundary doping of oxygen, Nat. Commun. 7 (2016). doi:10.1038/ncomms11225.

[26] J.M. Wheeler, V. Maier, K. Durst, M. Göken, J. Michler, Activation parameters for deformation of ultrafine-grained aluminium as determined by indentation strain rate jumps at elevated temperature, Mater. Sci. Eng. A. 585 (2013) 108–113. doi:10.1016/j.msea.2013.07.033.

[27] G. Sharma, A. Chatterjee, B. Paul, J. Varshney, J.K. Chakravartty, High temperature mechanical behavior of nanocrystalline Ni, Mater. Sci. Eng. A. 576 (2013) 69–73. doi:10.1016/j.msea.2013.03.068.

[28] G. Mohanty, J.M. Wheeler, R. Raghavan, J. Wehrs, M. Hasegawa, S. Mischler, L. Philippe, J. Michler, Elevated temperature, strain rate jump microcompression of nanocrystalline nickel, Philos. Mag. 95 (2014) 1878–1895. doi:10.1080/14786435.2014.951709.

[29] E. Hart, Theory of the tensile test, Acta Metall. 15 (1967) 351–355. doi:10.1016/0001-6160(67)90211-8.

[30] P.H. Pumphrey, H. Gleiter, The annealing of dislocations in high-angle grain boundaries, Philos. Mag. 30 (1974) 593–602. doi:10.1080/14786439808206584.

[31] A. Vorhauer, R. Pippan, On the onset of a steady state in body-centered cubic iron during severe plastic deformation at low homologous temperatures, Metall. Mater. Trans. A Phys. Metall. Mater. Sci. 39 (2008) 417–429. doi:10.1007/s11661-007-9413-1.

[32] S. Scheriau, Z. Zhang, S. Kleber, R. Pippan, Deformation mechanisms of a modified 316L austenitic steel subjected to high pressure torsion, Mater. Sci. Eng. A. 528 (2011) 2776–2786. doi:10.1016/j.msea.2010.12.023.

[33] A. Bachmaier, M. Hafok, R. Pippan, Rate Independent and Rate Dependent Structural Evolution during Severe Plastic Deformation, Mater. Trans. 51 (2010) 8–13. doi:10.2320/matertrans.MB200912.

[34] C.L. Wang, M. Zhang, T.G. Nieh, Nanoindentation creep of nanocrystalline nickel at elevated temperatures, J. Phys. D. Appl. Phys. 42 (2009) 115405. doi:10.1088/0022-3727/42/11/115405.

[35] J.M. Wheeler, D.E.J. Armstrong, W. Heinz, R. Schwaiger, High temperature nanoindentation: The state of the art and future challenges, Curr. Opin. Solid State Mater. Sci. 19 (2015) 354–366. doi:10.1016/j.cossms.2015.02.002.

[36] J.M. Wheeler, J. Michler, Elevated temperature, nano-mechanical testing in situ in the scanning electron microscope, Rev. Sci. Instrum. 84 (2013). doi:10.1063/1.4795829.

[37] W.C. Oliver, G.M. Pharr, Improved technique for determining hardness and elastic modulus using load and displacement sensing indentation experiments, J. Mater. Res. 7 (1992) 1564–1580.

doi:10.1557/JMR.1992.1564.

[38] B.N. Lucas, W.C. Oliver, The Elastic, Plastic and Time Dependent Properties of Thin Films as Determined by Ultra Low Load Indentation, Mater. Res. Soc. Symp. - Proc. 239 (1992) 337–341.

[39] V. Maier, K. Durst, J. Mueller, B. Backes, H.W. Höppel, M. Göken, Nanoindentation strain-rate jump tests for determining the local strain-rate sensitivity in nanocrystalline Ni and ultrafine-grained Al, J. Mater. Res. 26 (2011) 1421–1430. doi:10.1557/jmr.2011.156.

[40] K. Durst, V. Maier, Dynamic nanoindentation testing for studying thermally activated processes from single to nanocrystalline metals, Curr. Opin. Solid State Mater. Sci. 19 (2015) 340–353. doi:10.1016/j.cossms.2015.02.001.

[41] L.S. Toth, P. Gilormini, J.J. Jonas, Effect of rate sensitivity on the stability of torsion textures, Acta Metall. 36 (1988) 3077–3091. doi:10.1016/0001-6160(88)90045-4.

[42] O. V. Mishin, V.Y. Gertsman, R.Z. Valiev, G. Gottstein, Grain boundary distribution and texture in ultrafine-grained copper produced by severe plastic deformation, Scr. Mater. 35 (1996) 873–878. doi:10.1016/1359-6462(96)00222-9.

[43] Z.C. Wang, P.B. Prangnell, Microstructure refinement and mechanical properties of severely deformed Al-Mg-Li alloys, Mater. Sci. Eng. A. 328 (2002) 87–97. doi:10.1016/S0921-5093(01)01681-1.

[44] T. Hebesberger, H.P. Stüwe, A. Vorhauer, F. Wetscher, R. Pippan, Structure of Cu deformed by high pressure torsion, Acta Mater. 53 (2005) 393–402. doi:10.1016/j.actamat.2004.09.043.

[45] F. Wetscher, R. Pippan, Cyclic high-pressure torsion of nickel and Armco iron, Philos. Mag. 86 (2006) 5867–5883. doi:10.1080/14786430600838288.

[46] H.W. Zhang, X. Huang, N. Hansen, Evolution of microstructural parameters and flow stresses toward limits in nickel deformed to ultra-high strains, Acta Mater. 56 (2008) 5451–5465. doi:10.1016/j.actamat.2008.07.040.

[47] P. Ghosh, O. Renk, R. Pippan, Microtexture analysis of restoration mechanisms during high pressure torsion of pure nickel, Mater. Sci. Eng. A. 684 (2017) 101–109. doi:10.1016/j.msea.2016.12.032.

[48] E.O. Hall, Yield point phenomena in metals and alloys, Springer Science & Business Media, 2012.

[49] M. Göken, H.W. Höppel, T. Hausöl, J. Bach, V. Maier, C.W. Schmidt, D. Amberger, Grain refinement and deformation mechanisms in heterogeneous ultrafine- grained materials processed by accumulative roll bonding, in: Proc. 33rd Risø Symp. Mater. Sci. Nanometals - Status Perspect., 2012: pp. 31–48.

[50] M.-M. Primorac, M.D. Abad, P. Hosemann, M. Kreuzeder, V. Maier, D. Kiener, Elevated temperature mechanical properties of novel ultra-fine grained Cu–Nb composites, Mater. Sci. Eng. A. 625 (2015) 296–302. doi:10.1016/j.msea.2014.12.020.

[51] L. Priester, On the accommodation of extrinsic dislocations in grain boundaries, Interface Sci. 4 (1996) 205–219. doi:doi.org/10.1007/BF00240242.

[52] L. Priester, Grain Boundaries From Theory to Engineering, 1st ed., Springer Netherlands, 2013. doi:10.1007/978-94-007-4969-6.

[53] F. Mompiou, D. Caillard, M. Legros, H. Mughrabi, In situ TEM observations of reverse dislocation motion upon unloading in tensile-deformed UFG aluminium, Acta Mater. 60 (2012) 3402–3414. doi:10.1016/j.actamat.2012.02.049.

[54] A.A. Nazarov, Kinetics of grain boundary recovery in deformed polycrystals, Interface Sci. 8 (2000) 315–322. doi:10.1023/A:1008720710330.

[55] S. V. Divinski, G. Reglitz, H. Rösner, Y. Estrin, G. Wilde, Ultra-fast diffusion channels in pure Ni severely deformed by equal-channel angular pressing, Acta Mater. 59 (2011) 1974–1985. doi:10.1016/j.actamat.2010.11.063.

[56] S. V. Divinski, G. Reglitz, G. Wilde, Grain boundary self-diffusion in polycrystalline nickel of different purity levels, Acta Mater. 58 (2010) 386–395. doi:10.1016/j.actamat.2009.09.015.

[57] W. Chen, Z.S. You, N.R. Tao, Z.H. Jin, L. Lu, Mechanically-induced grain coarsening in gradient nano-grained copper, Acta Mater. 125 (2017) 255–264. doi:10.1016/j.actamat.2016.12.006.

[58] O. Renk, R. Pippan, Transition from thermally assisted to mechanically driven boundary migration and related apparent activation energies, Scr. Mater. 154 (2018) 212–215. doi:https://doi.org/10.1016/j.scriptamat.2018.05.052.

[59] O.D. Sherby, P.E. Armstrong, Prediction of activation energies for creep and self-diffusion from hot hardness data, Metall. Mater. Trans. B. 2 (1971) 3479–3484. doi:10.1007/BF02811630.

[60] J. Wang, Y. Iwahashi, Z. Horita, M. Furukawa, M. Nemoto, R.Z. Valiev, T.G. Langdon, An investigation of microstructural stability in an Al-Mg alloy with submicrometer grain size, Acta Mater. 44 (1996) 2973–2982. doi:10.1016/1359-6454(95)00395-9.

[61] T. Fujita, Z. Horita, T.G. Langdon, Characteristics of diffusion in Al-Mg alloys with ultrafine grain sizes, Philos. Mag. A Phys. Condens. Matter, Struct. Defects Mech. Prop. 82 (2002) 2249–2262. doi:10.1080/01418610208235736.

[62] X.F. Zhang, T. Fujita, D. Pan, J.S. Yu, T. Sakurai, M.W. Chen, Influences of grain size and grain boundary segregation on mechanical behavior of nanocrystalline Ni, Mater. Sci. Eng. A. 527 (2010) 2297–2304. doi:10.1016/j.msea.2009.12.005.

[63] A. Rajabzadeh, M. Legros, N. Combe, F. Mompiou, D.A. Molodov, Evidence of grain boundary dislocation step motion associated to shear-coupled grain boundary migration, Philos. Mag. 93 (2013) 1299–1316. doi:10.1080/14786435.2012.760760.

[64] A. Rajabzadeh, F. Mompiou, S. Lartigue-Korinek, N. Combe, M. Legros, D.A. Molodov, The role of disconnections in deformation-coupled grain boundary migration, Acta Mater. 77 (2014) 223–235. doi:10.1016/j.actamat.2014.05.062.

[65] J. Han, S.L. Thomas, D.J. Srolovitz, Grain-Boundary Kinetics: A Unified Approach, arXiv:1803.03214. (2018).

[66] T. Yu, D.A. Hughes, N. Hansen, X. Huang, In situ observation of triple junction motion during recovery of heavily deformed aluminum, Acta Mater. 86 (2015) 269–278. doi:10.1016/j.actamat.2014.12.014.

[67] S. Lartigue, L. Priester, Stability of extrinsic grain boundary dislocations in relation with intergranular segregation and precipitation, Acta Metall. 31 (1983) 1809–1819. doi:https://doi.org/10.1016/0001-6160(83)90127-X.

[68] W.A. Świątnicki, W. Łojkowski, M.W. Grabski, Investigation of grain boundary diffusion in polycrystals by means of extrinsic grain boundary dislocations spreading rate, Acta Metall. 34 (1986) 599–605. doi:10.1016/0001-6160(86)90175-6.

[69] M. Thuvander, M. Abraham, A. Cerezo, G.D.W. Smith, Thermal stability of electrodeposited nanocrystalline nickel and iron–nickel alloys, Mater. Sci. Technol. 17 (2001) 961–970. doi:10.1179/026708301101510799.

[70] Y.M. Wang, S. Cheng, Q.M. Wei, E. Ma, T.G. Nieh, A. Hamza, Effects of annealing and impurities on tensile properties of electrodeposited nanocrystalline Ni, Scr. Mater. 51 (2004) 1023–1028. doi:10.1016/j.scriptamat.2004.08.015.

[71] Y.D. Zheng, P.Q. Dai, W.C. Xu, S.R. Hu, Effect of annealing on tensile properties of electrodeposited nanocrystalline Ni with broad grain size distribution, Mater. Sci. Technol. 27 (2011) 1793–1797. doi:10.1179/026708311X13161822837811.

[72] O. Renk, A. Hohenwarter, B. Schuh, J.H. Li, R. Pippan, Hardening by annealing: Insights from different alloys, in: IOP Conf. Ser. Mater. Sci. Eng., 2015: p. 12043. doi:10.1088/1757-899X/89/1/012043.

[73] R. Kirchheim, Grain coarsening inhibited by solute segregation, Acta Mater. 50 (2002) 413–419. doi:10.1016/S1359-6454(01)00338-X.

[74] C.C. Koch, R.O. Scattergood, K.A. Darling, J.E. Semones, Stabilization of nanocrystalline grain sizes by solute additions, J. Mater. Sci. 43 (2008) 7264–7272. doi:10.1007/s10853-008-2870-0.

[75] M. Saber, C.C. Koch, R.O. Scattergood, Thermodynamic grain size stabilization models: An overview, Mater. Res. Lett. 3 (2015) 65–75. doi:10.1080/21663831.2014.997894.